An Improved VMD and Wavelet Hybrid Denoising Model for Wearable SSVEP-BCI

Yongquan Xia, Keyun Li, Duan Li, Jiaofen Nan, Ronglei Lu
School of Computer Science and Technology, Zhengzhou University of Light Industry, Zhengzhou, Henan, China

***Abstract*—The brain-computer interface (BCI) based on steady-state visual evoked potentials (SSVEP) has attracted considerable attention due to its non-invasiveness, low user training requirements, and efficient information transfer rate. To optimize the accuracy of SSVEP detection, we propose an innovative hybrid EEG denoising model combining variational mode decomposition (VMD) with wavelet packet transform(WPT). This model ingeniously integrates VMD decomposition and WPT denoising techniques, employing detrended fluctuation analysis (DFA) thresholding to deeply filter the noisy data collected from wearable devices. The filtered components are then reconstructed alongside the unprocessed components. Finally, three classification algorithms are used to validate the proposed method on a wearable SSVEP-BCI dataset. Our proposed algorithm achieves accuracies of 71.27% and 86.35% on dry and wet electrodes, respectively. Comparing the use of VMD combined with adaptive wavelet denoising and direct denoising with VMD, the classification accuracy of our method improved by 3.68% and 0.26% on dry electrodes, respectively, and by 3.28% and 0.66% on wet electrodes, respectively. The proposed approach demonstrates excellent performance and holds promising potential for application and generalization in the field of wearable EEG denoising.**

Keywords*—Brain-computer interface; steady-state visual evoked potential; style; variational mode decomposition; wavelet packet transform

I. INTRODUCTION

Brain-computer interface (BCI) technology facilitates the direct conversion of brain signals into computer input signals, enabling direct human-computer interaction [1, 2]. When neurons in the brain are active, they generate weak electrical signals, which can be transmitted through the scalp, skull, and tissues to the surface of the scalp, forming electroencephalogram (EEG) signals [3, 4]. Steady-state visual evoked potentials (SSVEP) [5] are among the most common neurophysiological electrical signals in EEG. Compared to other electrophysiological signal sources, SSVEP-based BCIs offer higher information transfer rate, signal-to-noise ratios, and classification accuracies. To enhance the practicality of SSVEP-based BCI systems, there is an increasing demand for wearable BCI systems.

EEG electrodes play a crucial role in wearable BCI systems. Dry electrodes, which do not require conductive gel, offer a convenient and durable method for EEG signal acquisition [6, 7]. However, due to the need for close contact with the scalp, dry electrodes often result in poorer signal quality and user experience. Additionally, portable devices are typically more susceptible to contamination from typical sources of noise compared to standard EEG systems [8-10]. Therefore, in wearable SSVEP-BCI data, noise reduction processing becomes particularly crucial.

The processing of wearable physiological signals remains a hot research topic, with significant achievements in the field of EEG denoising. Peng et al.[11] first proposed a novel model for removing eye artifacts from EEG signals, based on discrete wavelet transform (DWT) and adaptive noise cancellation (ANC). The results demonstrated the effectiveness of this model in removing eye artifacts, making it particularly suitable for applications in portable environments. Similarly, Zhao et al.[12] also introduced a hybrid denoising method using DWT and adaptive predictive filtering (APF) for automatic identification and removal of eye artifacts. However, some drawbacks of time-frequency transformation methods include limited resolution, windowing effects, occurrence of cross-terms, high complexity and computational costs, poor interpretability, sensitivity to noise, and challenges in parameter selection. EMD is an adaptive decomposition method that does not involve a complex selection process for basis functions. It offers higher resolution than traditional time-frequency analysis methods but suffers from drawbacks such as mode mixing, endpoint effects, and a lack of mathematical theory [13-15]. To overcome these limitations, improved EMD algorithms have been proposed, such as ensemble empirical mode decomposition (EEMD)[16] and complementary ensemble empirical mode decomposition (CEEMD) [17]. While these methods have improved the decomposition results, issues like mode mixing and endpoint effects persist, and all three methods lack mathematical theoretical support. In 2014, Dragomiretskiy and Rosso[18] introduced variational mode decomposition (VMD), which differs from EMD, EEMD, and CEEMD in that it is not "empirical" but rather supported by strong mathematical theory. VMD is a new adaptive signal decomposition algorithm and has shown promising results in denoising and time-frequency analysis [19-21].

However, a single time-frequency domain analysis methods lack uniformity in time-frequency resolution, making it challenging to accurately capture the changing characteristics of non-stationary signals across different time and frequency ranges. Subsequently, Narmada et al. [22] proposed a deep learning and heuristic-based adaptive pseudo-shadow wavelet denoising method, which enhances the denoising effect through a combination of EMD and DWT. Therefore, our study proposes a hybrid denoising technique combining VMD with wavelet packet transform (WPT), aiming to explore the intrinsic characteristics of SSVEP data. VMD, with its remarkable decoupling capability, effectively separates mixed components

in SSVEP signals. The wavelet-hybrid denoising technique effectively preserves the useful information in the signal while significantly attenuating the noise components, enhancing the purity of the signal.

To comprehensively validate the practicality of this approach, we employed three recognition algorithms: canonical correlation analysis (CCA), filter bank canonical correlation analysis (FBCCA), and task-related component analysis (TRCA). These algorithms, each with its unique features, classify and recognize signals from different perspectives, providing a comprehensive performance evaluation. Additionally, this paper further investigates the application potential of this method in wearable SSVEP EEG signal recognition by comparing it with different denoising methods.

The structure of the remaining part of this paper is as follows. The second part primarily elaborates on the methods used in this study. The third part provides an introduction to the dataset used and the determination of experimental parameters. The fourth part discusses relevant issues based on experimental results. Discussions continue in Section V. and the sixth part.summarize the work done in this paper.

II. METHOD

A. Overview

The workflow of this method includes the following steps: firstly, the EEG signals are subjected to initial preprocessing and bandpass filtering to eliminate noise interference. Next, the VMD technique is employed to decompose the signals into K band-limited intrinsic mode functions (BLIMFs), which helps better capture the frequency characteristics of the signals. Then, detrended fluctuation analysis (DFA) is utilized for threshold determination to filter out BLIMFs that do not meet the threshold conditions, which are subsequently subjected to wavelet denoising. Wavelet denoising mainly utilizes wavelet packet transform (WPT), effectively reducing noise components in the signals. Finally, the reconstructed signals obtained by adding the threshold-filtered BLIMFs and further processed BLIMFs are inputted into three different classification algorithms for further recognition and classification, as illustrated in Fig. 1.

B. VMD and Wavelet Hybrid Denoising

1) Variational mode decomposition: Variational mode decomposition (VMD) is a novel and more effective non-recursive signal preprocessing algorithm that can adaptively determine relevant frequency bands and compute individual mode components simultaneously. The VMD algorithm decomposes any signal x(t) into K discrete sub-signals or modes u_k, where each mode is centered around its respective central frequency ω_k. The expression for u_k is given in Equation (1):

$$u_k(t) = A_k(t)\cos\left(\omega_k(t)\right) \tag{1}$$

In the equation, $u_k(t)$ represents the k-th intrinsic mode function (IMF), which is primarily designed to limit bandwidth; $A_k(t)$ denotes the instantaneous amplitude of $u_k(t)$; $\omega_k(t)$ stands for the instantaneous frequency of $u_k(t)$. Each component is centered around the central frequency $\omega_k(t)$, and gaussian smoothing can be employed to estimate the bandwidth. Due to the sparsity of VMD decomposition, the decomposition problem can be formulated as follows. As shown in Equation (2):

$$\begin{aligned} &\min_{\{u_k\},\{\omega_k\}} \left\{ \sum_{k=1}^{K} \left\| \partial_t \left[\left(\delta(t) + \frac{j}{\pi t} \right) * u_k(t) \right] e^{-j\omega_k t} \right\|_2^2 \right\} \\ &s.t. \sum_{k=1}^{K} u_k(t) = x \end{aligned} \tag{2}$$

In the equation, t denotes the time symbol, δ(t) represents the dirac delta function, * denotes convolution. To solve the aforementioned problem optimally, an augmented lagrangian function is introduced, transforming the constrained variational problem into an unconstrained variational problem, expressed as:

$$\begin{aligned} L\left(\{u_k\},\{\omega_k\},\lambda\right) &= \alpha \sum_{k=1}^{K} \left\| \partial_t \left[\left(\delta(t) + \frac{j}{\pi t} \right) * u_k(t) \right] e^{-j\omega_k t} \right\|_2^2 \\ &+ \left\| x(t) - \sum_{k=1}^{K} u_k(t) \right\|_2^2 + \left\langle \lambda(t), x(t) - \sum_{k=1}^{K} u_k(t) \right\rangle \end{aligned} \tag{3}$$

In the equation, α is a secondary penalty factor ensuring signal reconstruction accuracy; λ(t) represents the Lagrange multiplier operator. Equation (3) is then solved using the alternating direction method of multipliers (ADMM). In the fourier domain, the optimal $u_k(\omega)$ is directly updated via wiener filtering [23].Therefore, wiener filtering is embedded in VMD to enhance its robustness to sampling and noise. This yields the time-domain mode $u_k(t)$:

$$\hat{u}_k^{n+1}(\omega) = \frac{\hat{x}(\omega) - \sum_{i \neq k} \hat{u}_i(\omega) + \frac{\hat{\lambda}(\omega)}{2}}{1 + 2\alpha(\omega - \omega_k)^2} \tag{4}$$

$$\hat{u}_k(t) = \Re\left\{ ifft\left(\hat{u}_k(\omega)\right) \right\} \tag{5}$$

Where $\hat{x}(\omega)$ is the fourier transform of the signal $x(t)$, $ifft(\cdot)$ is the inverse fourier transform of, and $\Re\{\cdot\}$ denotes the real part of the analytical signal. The updated equation for ω_k is as follows, and its optimization is also performed in the fourier domain. As shown in Equation (6):

$$\omega_k^{n+1} = \frac{\int_0^\infty \omega \left|\hat{u}_k(\omega)\right|^2 d\omega}{\int_0^\infty \left|\hat{u}_k(\omega)\right|^2 d\omega} \tag{6}$$

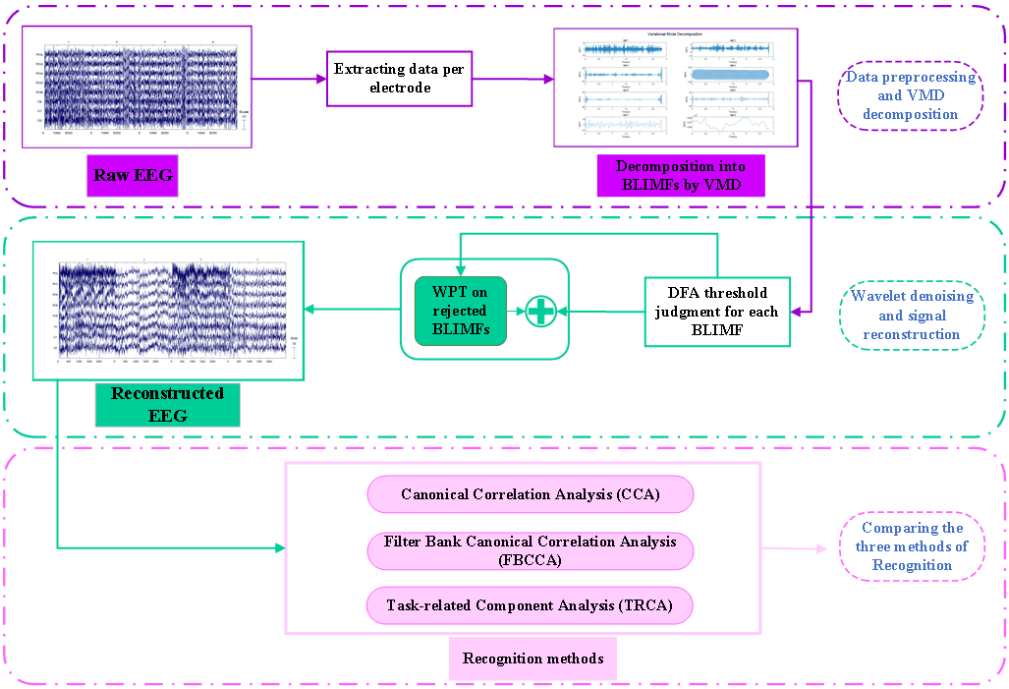

Fig. 1. Overall workflow diagram.

In VMD decomposition, the penalty factor α and the number of mode components K directly influence the decomposition results. α primarily affects the accuracy of the decomposition results, while the value of K directly affects the correctness of the decomposition results. If the chosen K is smaller than the number of useful components in the signal (under-decomposition), it may lead to incomplete decomposition and mode mixing. Conversely, if the chosen K is greater than the number of useful components in the signal (over-decomposition), it may result in some irrelevant false components. Therefore, the selection of K is crucial for the results of VMD.

2) The principle of VMD and wavelet hybrid denoising: Wavelet packet transform (WPT) is an advancement built upon the foundation of DWT. In DWT, a signal is decomposed into a series of high-frequency and low-frequency components, but only the low-frequency part is iteratively decomposed. In contrast, WPT simultaneously decomposes both high-frequency and low-frequency components at each decomposition level. This means that it can analyze the frequency content of the signal in more detail. Wavelet packets inherit the advantages of wavelet transform, capturing both time-domain and frequency-domain features, which enables effective handling of unstable signals. Additionally, for both high-frequency and low-frequency signal components, wavelet packet transform provides good signal processing performance while maintaining the same time-frequency resolution. The full-band analysis capability of WPT is particularly suitable for applications where signal characteristics are not limited to the low-frequency range alone. Due to its fine-grained analysis characteristics, wavelet packet decomposition demonstrates its unique advantages in various applications. It not only offers improved performance in signal denoising and data compression but also exhibits unparalleled capabilities in biomedical signal processing, speech recognition, and seismic data analysis [24-27].

In the method proposed in this paper, after decomposing the modal components using VMD, a threshold judgment is applied to these components. Components that do not meet the threshold condition are further denoised using WPT. In the process of wavelet denoising, the selection of appropriate wavelet functions and decomposition levels is crucial. Previous research [28] has shown that the wavelet function 'db8' has more effective denoising effects for EEG signals from healthy subjects. However, to more accurately select wavelet functions suitable for EEG signals, this paper refers to the method in [29] and tries different Daubechies wavelet functions. The experimental results show that 'db4' and 'db8' have more significant denoising effects on EEG signals. Therefore, 'db4' was chosen as the wavelet function suitable for the experiment. For determining the decomposition levels, this paper follows the definition of decomposition levels based on Shannon entropy [30]. The process involves increasing the decomposition levels and then calculating the entropy of the detail coefficients and approximation coefficients. When the detail entropy is greater than the approximation entropy, the decomposition level at which to stop is determined. Based on experimental results, the decomposition level was determined to be 3. Finally, the denoised components obtained through wavelet denoising are added to the components that meet the threshold conditions to reconstruct cleaner EEG signals.

C. The Three Recognition Algorithms

This paper mainly employs three recognition algorithms, namely CCA, FBCCA, and TRCA, to classify wearable SSVEP EEG signals.

1) Canonical correlation analysis (CCA): The canonical correlation analysis (CCA) algorithm is a multivariate statistical analysis method that utilizes the correlation between composite variables to reflect the overall correlation between two sets of indicators. It is widely used in the analysis of SSVEP signals due to its effectiveness and robustness [31].

2) Filter bank canonical correlation analysis (FBCCA): Due to non-Gaussian background noise and its harmonics affecting SSVEP, the CCA method may not fully utilize the characteristics of SSVEP signals [32]. To address this issue, Chen et al. proposed FBCCA [33], which combines filter bank technology with CCA to enhance performance.*Task-related component analysis (TRCA)*: The TRCA algorithm was first proposed by Nakanishi in 2018 [34]. It aims to enhance the signal-to-noise ratio and suppress spontaneous brain activity by maximizing the repeatability of inter-trial covariance using training data from target subjects, thereby extracting task-related components.

Assuming $X_i^k \in \mathbb{R}^{N_c \times N_s}$ and $X_j^k \in \mathbb{R}^{N_c \times N_s}$ represent the EEG signals of the i-th and j-th experiments corresponding to the k-th stimulus frequency for a particular subject, where N_c denotes the number of EEG channels, N_s denotes the number of sampling points, and k=1,2,…,N_f, the constrained optimization problem of TRCA is reduced to the following Rayleigh-Ritz eigenvalue problem. As shown in Equation (7):

$$w = \arg\max_{w} \frac{w^T S w}{w^T Q w} \tag{7}$$

Where S and Q are respectively the sums of inter-trial covariance matrix and auto-covariance matrix, calculated as follows:

$$S = \sum_{\substack{i,j=1 \\ i \neq j}}^{N_b} Cov(X_i^k, X_j^k) \tag{8}$$

$$Q = \sum_{\substack{i,j=1 \\ i = j}}^{N_b} Cov\left(X_i^k, X_j^k\right) \tag{9}$$

Where N_b is the number of training experiments.

The spatial filters can be obtained from the eigenvectors corresponding to the largest eigenvalue of the matrix $Q^{-1}S$. Therefore, spatial filters corresponding to all stimulus frequencies can be computed. The correlation coefficient r_k between the test data $X_t = \mathbb{R}^{N_c \times N_s}$ and the averaged training template $\bar{X}_k$ is calculated by the following equation:

$$r_k = \rho\left(X_t^T W, \bar{X}_k^T W\right) \tag{10}$$

Then, the maximum correlation coefficient among all correlation coefficients with the averaged training templates for all stimulus frequencies is found. The stimulus frequency corresponding to the maximum correlation coefficient is identified as the target stimulus.

D. Performance Evaluation

This paper evaluates the performance of the model using accuracy and F_1score based on the confusion matrix. The expressions for accuracy and F_1score are as follows:

$$\text{Accuracy} = \frac{TP + TN}{TP + FP + FN + TN} \tag{11}$$

$$\text{Precision} = \frac{TP}{TP + FP} \tag{12}$$

$$\text{Recall} = \frac{TP}{TP + FN} \tag{13}$$

$$\text{F}_1\text{score} = 2 \times \frac{\text{Precision} \times \text{Recall}}{\text{Precision} + \text{Recall}} \tag{14}$$

where TP, TN, FP, and FN represent true positive, true negative, false positive,and false negative, respectively.

III. Dataset and Parameter Settings

A. Dataset

The proposed method model was validated on a wearable SSVEP-BCI dataset [35]. The dataset comprised 102 healthy subjects with normal or corrected-to-normal vision (64 males, 38 females, aged 8-52 years) recorded using SSVEP-based brain-computer interface, involving 12 targets. The 12 targets were encoded using the JFPM method, with a frequency range of 9.25 to 14.75 Hz in 0.5 Hz intervals, and a phase difference of 0.5 π between adjacent targets. For each subject, experiments were conducted using both dry and wet electrodes, with 10 consecutive data blocks recorded for each electrode type. Each block contained 12 trials corresponding to each target displayed once in random order. Data were recorded according to the international 10-20 system, with 8 electrodes placed on the parieto-occipital area (POz, PO3, PO4, PO5, PO6, Oz, O1, O2) and 2 electrodes on the frontal area serving as reference and ground. Data extraction from the public dataset was performed at time points ranging from 0.64 to 2.64 seconds during the experiment (including 0.5 seconds before stimulus onset, 0.14 seconds of visual delay, 2 seconds of stimulus presentation, and 0.2 seconds after stimulus offset), with the first 20 subjects participating in our study.

B. Experimental Environment and Parameter Settings

The method proposed in this study has been implemented in MATLAB 2022b. To effectively utilize wavelet processing functions, the MATLAB environment in the research setup has been installed with the Time-Frequency Analysis Toolbox (TFA-Toolbox).

1) Method for determining the number of modes K in VMD: Before conducting experiments, it is necessary to determine the number of modes K for VMD decomposition. In previous literature, the number of modes K is typically defined using the same number of EMD decompositions and wavelet packet decompositions [36], or selected by calculating the scaling exponent α of the input signal [23]. However, the aforementioned techniques have certain limitations when

dealing with experiment signals with complex frequency components. In this study, the energy difference principle is used as an auxiliary algorithm, with the experimental results of classification accuracy as the main basis, combined with the analysis of decomposition results to determine the value of K.

Energy Difference Principle: VMD utilizes a variational framework-based constrained variational model to decompose signals, and the components obtained from the decomposition have orthogonal relationships in terms of energy. In other words, the sum of the energies of each component should be equal to the energy of the original signal, which adheres to the energy difference principle. If K is set too large, it will lead to over-decomposition of the signal, resulting in spurious components and causing the sum of energies of the components generated by over-decomposition to exceed the sum of energies of the components generated by normal decomposition. Therefore, the optimal value of the parameter K for VMD can be determined by comparing energy differences. The formula for calculating signal energy is as follows:

$$E = \sqrt{\frac{\sum_{i=1}^{n} y^2(i)}{n}} \tag{15}$$

In the formula, E represents the energy of the signal; y(i) represents the EEG signal sequence; n represents the number of sampling points. The formula for calculating the energy difference is as follows:

$$\eta = \frac{|E_K - E_{K-1}|}{E_{K-1}} \tag{16}$$

According to equation (16), η represents the difference between E_K and E_{K-1}. A larger value of η indicates a more pronounced over-decomposition phenomenon in VMD, whereas a smaller value of η may suggest under-decomposition of the signal. For non-stationary and complex signals such as EEG signals, η typically remains near small values under conditions of under-decomposition or appropriate decomposition. With an increase in the parameter K, the over-decomposition phenomenon causes η to significantly increase. Therefore, the value of K at the inflection point can be considered as an effective number of modes for VMD decomposition.

First, use FBCCA to classify the original EEG data to obtain the classification accuracy of dry and wet electrodes as a reference. Then, reconstruct the signal and perform classification under different numbers of modes, observing the results and analyzing the appropriate range of K values. In addition, with a step size of 0.5 seconds, gradually select data lengths of 0.5 seconds, 1 second, 1.5 seconds, and 2 seconds. The specific classification accuracies are shown in Table I (the upper part represents the results for dry electrodes, and the lower part represents the results for wet electrodes):

From Table I, it can be observed that the appropriate value of K is approximately around 20. In order to determine the value of K more precisely and accurately, the energy difference principle is used. The experiment is conducted using data from the same participant, and the results are shown in Table II.

From the results in Table II, it can be observed that analyzing the values of η reveals that when K=20, η suddenly increases, while other modal values remain approximately around 0.01. Therefore, based on the energy difference principle, the optimal choice for K is determined to be 20. Considering the comprehensive analysis above, the value of K in the proposed method should be set to 20 to ensure that the data can be accurately decomposed.

2) DFA Threshold Determination Method: In the proposed method in this paper, a reliable threshold is needed to select the obtained different mode functions after VMD decomposition. Since these decomposed components also contain noise, the Hurst exponent is used to determine whether there is noise in the obtained BLIMFs[30].

In non-stationary time series, estimating the hurst exponent can be challenging as certain methods may yield misleading results. Considering the non-stationary nature of wearable EEG signals, traditional approaches may not be suitable. However, detrended fluctuation analysis (DFA) possesses the capability to detrend time series, making it an ideal choice for estimating the hurst exponent. Therefore, this paper employs the DFA method aiming to accurately reveal the scaling properties of the signal and detect its long-range correlations, thereby providing a deeper understanding of the dynamic nature of wearable EEG signals. The steps for computing the hurst exponent using DFA are outlined in Algorithm 1.

Based on the DFA thresholding process (see Fig. 2), BLIMFs that meet the threshold criteria are retained, while those that do not meet the threshold criteria undergo further wavelet denoising. Finally, these two components are added together to generate a cleaner EEG signal. In this process, the parameter α represents the scaling exponent, playing a crucial role in measuring the roughness of the sequence. According to the empirical findings in [30], to address potential mode mixing issues, α is set to 0.75 in this study.

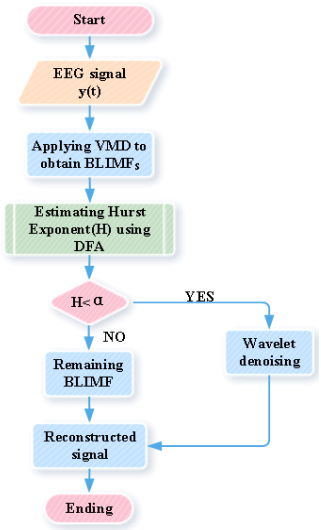

Fig. 2. Flowchart of DFA threshold determination

IV. Experimental Results

A. Recognition Results based on the Proposed Method in this Paper

First, the EEG data are directly processed using CCA, FBCCA, and TRCA as reference algorithms to obtain classification accuracy. Subsequently, the data are divided into dry and wet electrodes for each channel and fed into the proposed model. The data undergo bandpass and notch filtering, followed by VMD decomposition with a mode number of 20. Then, DFA thresholding is applied to determine which mode components do not meet the threshold criteria. These components undergo wavelet denoising, primarily using WPT for experimentation. Finally, the denoised components are added to the components that meet the threshold criteria to reconstruct a clearer EEG signal. The reconstructed signals are classified using the three recognition algorithms. Recordings of recognition results are made using data lengths of 0.5s, 1s, 1.5s, and 2s, as shown in Tables III and IV.

TABLE I. Classification Accuracy (MEAN ± STD %)

Method	Data length(s)			
	0.5	1	1.5	2
FBCCA	15.17±9.38 22.17±10.66	29.46±16.39 48.71±19.87	44.38±20.44 66.58±21.77	58.42±22.14 76.29±20.04
VMD+FBCCA(Modes)				
K=5	12.29±4.95 16.83±8.99	23.42±14.02 33.75±17.48	35.50±19.38 49.17±20.62	47.46±21.56 60.62±21.80
K=10	13.33±8.12 20.17±10.19	27.42±18.81 46.33±17.83	43.00±21.85 62.92±22.33	56.33±23.14 74.08±20.72
K=15	15.08±8.75 22.71±9.71	29.12±16.48 47.25±19.10	44.79±21.39 66.83±19.64	59.29±22.30 76.46±19.68
K=20	15.20±8.75 23.79±9.71	32.12±17.48 52.25±18.10	46.79±19.35 68.83±18.64	61.23±21.30 80.01±16.68
K=25	15.02±8.78 21.99±9.76	28.87±16.31 48.67±19.73	45.57±21.87 67.33±20.11	60.69±22.59 78.46±18.65

TABLE II. Values of H Under Different Numbers of Modes

Modes	η
K=18	0.0092
K=19	0.0106
K=20	0.0213
K=21	0.0158
K=22	0.0067

Algorithm 1: DFA steps for calculating the Hurst index

1. Sequence normalization: For a given time series X, first calculate its cumulative time series as shown in the fol lowing equation:

$$Y(i) = \sum_{k=1}^{i} X(k) - \mu \quad (17)$$

where μ is the mean value of the sequence X.

2. Segmentation to compute the mean: The cumulative time series Y is divided into different time windows (or sc ales), often called boxes, each of length n.

3. Linear fitting: For each window, find the trend of the sequence Y(i) within that window by least squares linear f itting.

4. Calculate the root mean square deviation: Calculate the deviation between the actual data and the fitted line in each window, which is often referred to as "fluctuation".

5. Fit a straight line: for different window lengths, the relationship between fluctuations and window length is plot ted as a logarithmic plot, a straight line is fitted to this image, and its slope is calculated, the slope is the Hurst inde x.

TABLE III. EXPERIMENTAL RESULTS OF DIRECTLY USING RECOGNITION ALGORITHMS (MEAN ± STD %)

Method	Data length(s)	Electrode type	Accuracy(%)	F_1
CCA	0.5	dry wet	11.25±9.78 16.67±10.70	8.88 14.97
	1	dry wet	26.25±17.68 41.04±20.59	22.71 38.86
	1.5	dry wet	41.25±19.67 56.87±26.88	38.52 55.77
	2	dry wet	52.29±21.55 66.46±25.57	49.94 64.96
FBCCA	0.5	dry wet	15.17±9.38 22.17±10.66	14.34 21.04
	1	dry wet	29.46±16.39 48.71±19.87	28.34 47.23
	1.5	dry wet	44.38±20.44 66.58±21.77	43.19 64.96
	2	dry wet	58.42±22.14 76.29±20.04	57.36 75.08
TRCA	0.5	dry wet	21.86±12.01 52.14±19.01	19.23 50.26
	1	dry wet	45.37±19.30 73.48±23.10	44.39 71.04
	1.5	dry wet	60.25±20.38 79.35±22.49	59.06 77.30
	2	dry wet	66.47±21.58 82.47±22.72	65.38 80.58

TABLE IV. EXPERIMENTAL RESULTS OF THE PROPOSED METHOD (MEAN ± STD %)

Method	Data length(s)	Electrode type	Accuracy(%)	F_1
CCA	0.5	dry wet	13.29±9.90 17.00±10.72	11.16 15.61
	1	dry wet	28.75±18.53 42.71±19.31	23.37 40.68
	1.5	dry wet	43.08±18.30 60.42±23.18	38.36 58.51
	2	dry wet	53.25±22.29 69.58±23.54	50.02 68.06
FBCCA	0.5	dry wet	16.01±9.12 23.42±9.75	15.21 22.31
	1	dry wet	32.50±16.65 51.79±18.96	31.51 50.48
	1.5	dry wet	49.04±21.94 72.46±18.40	48.09 71.22
	2	dry wet	63.08±23.42 80.58±16.88	62.12 79.66
TRCA	0.5	dry wet	23.57±14.71 55.39±20.04	21.37 53.98
	1	dry wet	48.59±22.38 76.28±21.45	47.59 75.49
	1.5	dry wet	63.19±21.20 83.58±18.38	61.38 81.05
	2	dry wet	71.27±20.49 86.35±16.19	70.21 84.20

From the experimental results in Table III and Table IV, it can be observed that after applying the VMD and WPT hybrid denoising method, the three recognition methods show improvements across different data lengths. For instance, at 2 seconds, the classification accuracy of CCA for dry and wet electrodes was initially 52.29% and 66.46%, respectively. After denoising, the classification accuracy increased to 53.25% and 69.58%, respectively, representing improvements of 0.96% and 3.12%, respectively. Similarly, for FBCCA at 2 seconds, the classification accuracy for dry and wet electrodes increased by 4.66% and 4.29%, respectively, while for TRCA, the increase was 4.8% and 3.88%, respectively. This indicates a significant improvement, especially for dry electrodes, validating the superiority of the denoising method proposed in this paper. The experimental results of the proposed method are visualized in Fig. 3.

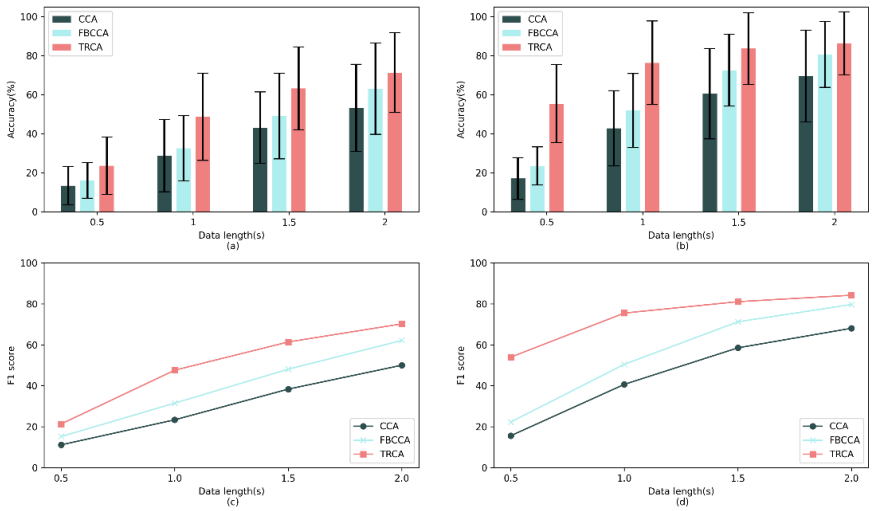

Fig. 3. Illustrates the results obtained based on the method proposed in this paper: (a) represents the classification accuracy for dry electrodes, (b) represents the classification accuracy for wet electrodes, (c) represents the F_1score for dry electrodes, (d) represents the F_1score for wet electrodes

From Fig. 3, it can be observed that TRCA shows significant improvements in classification accuracy and F1 score for dry and wet electrodes at data lengths of 1 second and 1.5 seconds. At 2 seconds, the classification accuracy for dry and wet electrodes reaches 71.27% and 86.35%, respectively.

B. Comparing Different Denoising Methods

To further denoise the BLIMFs obtained from VMD decomposition, this section compared the effectiveness of three different denoising methods: adaptive wavelet thresholding, removal of the highest and lowest frequency components, and DFA thresholding combined with wavelet packet transform (WPT).

Firstly, adaptive wavelet denoising was applied to the BLIMFs obtained from VMD decomposition. This method dynamically adjusts the noise filter based on the signal characteristics, allowing for finer noise reduction. The wavelet function 'db4' was chosen, with a decomposition level of 3, and the threshold was adaptively selected using the 'Rigrsure' method. Secondly, spectral analysis was conducted on the decomposed BLIMFs components to remove the highest and lowest frequency components, aiming to eliminate noise caused by extreme frequency components. In contrast, the method proposed in this paper, which combines DFA thresholding with WPT, provides a more detailed treatment of the signal's frequency characteristics. WPT also utilizes the 'db4' wavelet function, with a decomposition level of 3. The resulting classification accuracy and F_1score are presented in Tables V and VI, respectively, while the visualizations are depicted in Fig. 4 and 5.

TABLE V. EXPERIMENTAL RESULTS USING VMD WITH ADAPTIVE WAVELET DENOISING

Method	Data length(s)	Electrode type	Accuracy(%)	F_1
CCA	0.5	dry wet	11.04±9.34 16.25±8.11	9.18 15.23
	1	dry wet	25.21±17.65 43.96±18.56	21.12 41.85
	1.5	dry wet	42.08±21.57 59.58±23.79	38.43 57.37
	2	dry wet	53.33±22.38 66.79±24.84	50.81 64.71
FBCCA	0.5	dry wet	14.29±7.75 19.79±9.58	13.69 18.58
	1	dry wet	29.50±16.11 45.42±18.02	28.67 43.97
	1.5	dry wet	46.21±20.44 65.79±19.66	45.32 64.38
	2	dry wet	60.46±22.58 76.98±18.72	59.67 74.01
TRCA	0.5	dry wet	20.19±12.34 53.29±20.04	19.27 51.23
	1	dry wet	46.39±20.03 74.48±22.38	45.38 73.30
	1.5	dry wet	61.89±20.35 81.59±19.29	60.28 80.02
	2	dry wet	67.59±21.38 83.07±18.58	66.07 81.36

TABLE VI. EXPERIMENTAL RESULTS USING VMD WITH DIRECT REMOVAL OF HIGH AND LOW COMPONENTS

Method	Data length(s)	Electrode type	Accuracy(%)	F_1
CCA	0.5	dry wet	13.12±9.15 14.79±6.38	11.52 13.30
	1	dry wet	26.67±17.55 47.08±18.87	23.90 44.21
	1.5	dry wet	47.29±21.13 66.46±22.46	45.08 65.04
	2	dry wet	58.13±21.31 73.54±21.74	55.92 71.98
FBCCA	0.5	dry wet	15.20±8.38 20.62±9.40	14.45 19.29
	1	dry wet	30.42±15.80 46.67±18.30	29.63 45.31
	1.5	dry wet	47.62±20.96 67.00±19.63	46.53 65.58
	2	dry wet	60.79±23.25 77.08±18.82	59.84 74.91
TRCA	0.5	dry wet	22.38±13.49 56.58±20.48	20.38 54.13
	1	dry wet	48.41±22.31 74.39±22.19	46.98 73.27
	1.5	dry wet	64.02±21.15 84.48±18.12	63.07 81.25
	2	dry wet	71.01±20.18 85.69±17.68	70.11 83.21

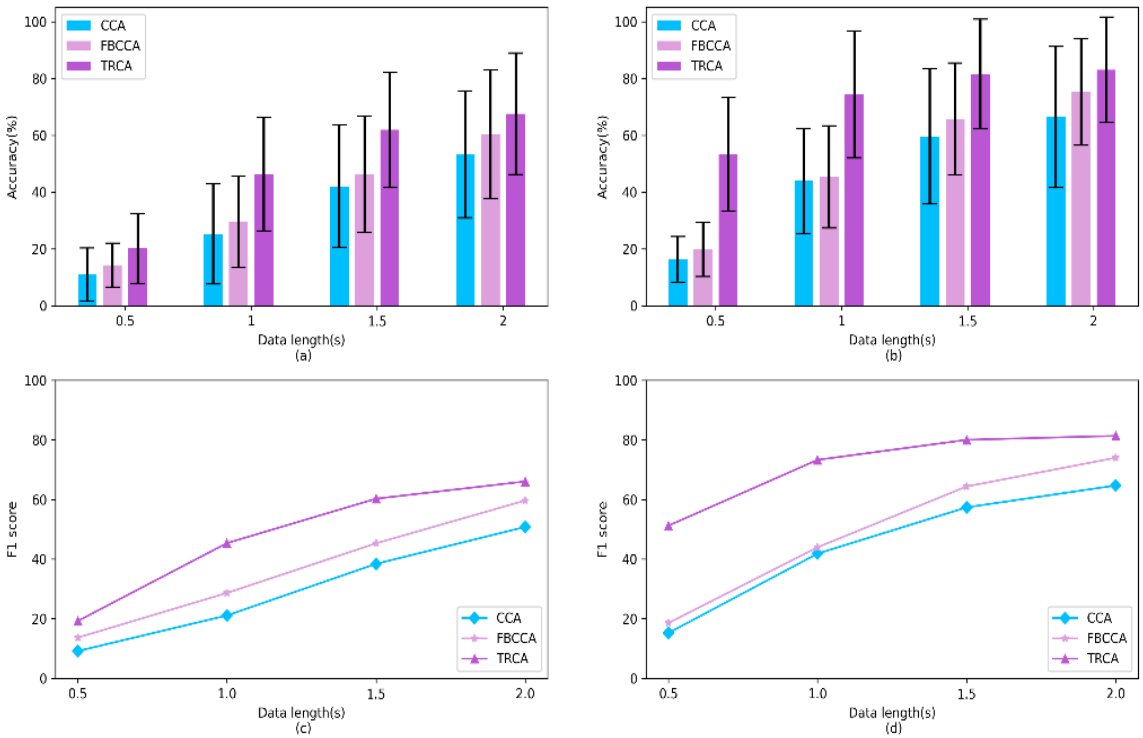

Fig. 4. Experimental results using VMD withadaptive wavelet thresholding: (a) represents the classification accuracy for dry electrodes, (b) represents the classification accuracy for wet electrodes, (c) represents the F_1score for dry electrodes, (d) represents the F_1score for wet electrodes

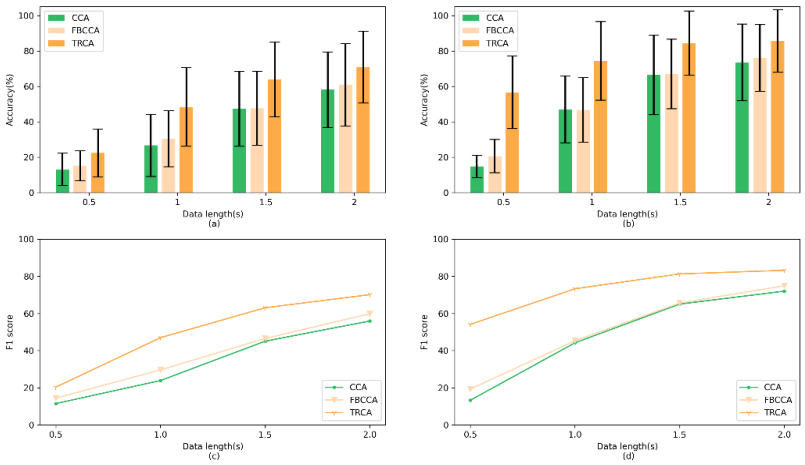

Fig. 5. Experimental results using VMD with direct removal of high and low components: (a) represents the classification accuracy for dry electrodes, (b) represents the classification accuracy for wet electrodes, (c) represents the F_1score for dry electrodes, (d) represents the F_1score for wet electrodes

From the above results, it can be observed that compared to directly using the three recognition algorithms, using VMD with adaptive wavelet denoising and direct removal of high and low components both resulted in increased classification accuracy and F_1score. However, neither of these denoising methods achieved the effectiveness of using VMD with WPT.

V. Discussion

To visually demonstrate the increase in classification accuracy achieved by different denoising methods compared to not using any denoising method, three approaches were set as follows: using VMD combined with adaptive wavelet denoising as Method 1, employing VMD with direct removal of high and low-frequency components as Method 2, and utilizing VMD combined with WPT as Method 3. As shown in Fig. 6, the left side illustrates the increase in classification accuracy for dry electrodes after applying different denoising methods, while the right side reflects the improvement for wet electrodes. Through this comparison, we can clearly observe the enhancement effect of various denoising methods on classification accuracy, thereby providing a more accurate evaluation of the effectiveness of different denoising strategies.

From Fig. 6, it can be observed that the increase in classification accuracy for dry and wet electrodes is highest when using Method 2 of denoising, especially for the CCA recognition algorithm. However, for the FBCCA and TRCA algorithms, the highest increase is observed when using Method 3. The reason for the significant increase in classification accuracy after applying Method 2, particularly for the CCA recognition algorithm, lies in its ability to selectively eliminate noise interference, thereby enhancing the accuracy of signal synchronization detection and complementing the performance of the CCA algorithm.

This study primarily employs VMD for signal decomposition to demonstrate its superiority. Additionally, to delve into the impact of different decomposition methods on wearable EEG data, the data of the same subject are decomposed using EMD, EEMD, CEEMD, and VMD. Subsequently, WPT is uniformly applied for wavelet denoising, and the denoised signals are reconstructed. Fig. 7 illustrates the power spectral density plots of these four decomposition methods, depicting the data from all samples of dry and wet electrodes of subject 5 at a stimulus frequency of 11.25 Hz.

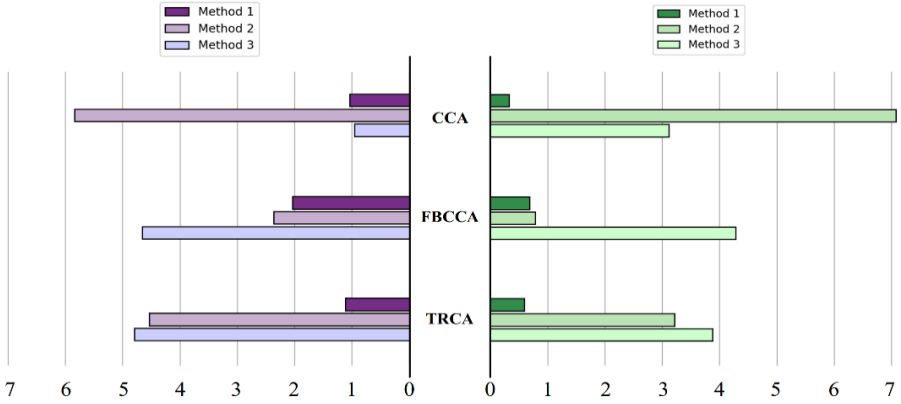

Fig. 6. Increase in classification accuracy

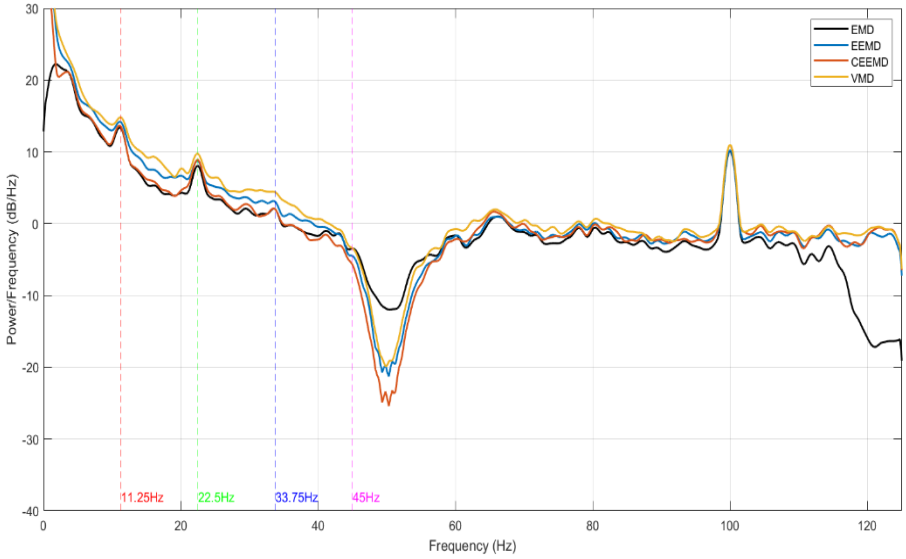

Fig. 7. Power spectral density plots of different decomposition methods

Firstly, it is noticeable that the power spectral density of the signal decomposed and reconstructed using VMD is relatively higher at the stimulus frequency and its first, second, and even third harmonics. This indicates that VMD effectively preserves the characteristics of the original signal at these specific frequencies during decomposition. As an adaptive signal decomposition method, VMD seeks the optimal mode functions to match the intrinsic features of the signal, demonstrating its superiority in handling complex signals.Additionally, it can be observed that the power spectral density of signals decomposed using EEMD is relatively higher compared to CEEMD. This difference may arise from the distinct decomposition strategies employed by these methods. EEMD aids decomposition by adding white noise, effectively suppressing mode mixing phenomena and enhancing decomposition accuracy. On the other hand, CEEMD, an improved version of EEMD, further reduces reconstruction errors and mode mixing by introducing the concept of complete ensemble. However, in some cases, CEEMD may sacrifice the preservation of certain signal features due to its emphasis on noise and mixing elimination. While VMD, EEMD, and CEEMD are all effective methods for handling complex signals, they may exhibit different strengths and limitations depending on the nature of the signal being processed. In practical applications, it is essential to select the appropriate signal decomposition method based on the specific characteristics and requirements of the signal to obtain the most accurate and meaningful results. Moreover, the phenomenon where CEEMD performs less effectively than EEMD in certain cases warrants further research and exploration for optimization and improvement in future work. Comparing the results of our study on wearable SSVEP EEG data with existing research, in reference [37], FBCCA was used for classification on 2-second data lengths, yielding classification accuracies of 59.3% and 77.9% for dry and wet electrodes, respectively. In contrast, our proposed method significantly improves these results, achieving 3.78% and 2.68% higher classification accuracies for dry and wet electrodes using the same FBCCA classification. In reference [38], TRCA, Compact-CNN, Conv-CA, and DNN were used, resulting in classification accuracies of 83.17%, 52.20%, 82.24%, and 71.42% for wet electrodes at the longest data length. In comparison, our method using denoising and TRCA classification improved wet electrode classification accuracies by 3.18%, 34.15%, 4.11%, and 14.93%, respectively. Our study provides a detailed comparison of methods at different stages, discussing their strengths and weaknesses, offering valuable reference and guidance for further research in wearable EEG signal processing.

VI. Conclusions

The paper proposes a denoising method combining Variational Mode Decomposition (VMD) with wavelet transformation and applies it to the recognition task of wearable SSVEP (Steady-State Visual Evoked Potential) brainwave signals. To validate the effectiveness of this method, the experiments are divided into two core parts. In the first part, three classification algorithms, namely CCA, FBCCA, and TRCA, are directly applied to identify the original signals, and their classification accuracy and F_1score are recorded. Subsequently, these results are compared with the recognition results of signals processed using the denoising method proposed in this paper. Experimental results show that, after applying the denoising method proposed in this paper, the performance of the three classification algorithms improved significantly across different data lengths. The TRCA recognition algorithm achieved the highest classification accuracy for both dry and wet electrodes, reaching 71.27% and 86.35%, respectively. In the second part of the experiment, the performance of various denoising methods is further compared, including the adaptive wavelet threshold method, the removal of extreme frequency components (high and low frequencies), and the threshold judgment combined with Wavelet Packet Transform (WPT) denoising method proposed in this paper. The core of the proposed method lies in preserving the useful feature information in the decomposed components through fine threshold judgment. The experimental results show that, whether for SSVEP brainwave signals collected from dry electrodes or wet electrodes, the denoising method proposed in this paper exhibits excellent classification accuracy and F_1score.

In summary, the denoising method combining VMD with wavelet transformation proposed in this paper not only effectively improves the recognition performance of wearable SSVEP brainwave signals but also has certain generalization and application value, providing new ideas and methods for research and practice in related fields. Our next steps will involve exploring additional classification algorithms, optimizing denoising parameters, and processing longer duration data to further enhance recognition performance and broaden applicability.

DATA AVAILABILITY STATEMENT

The dataset used in our study is available at the following link: http://bci.med.tsinghua.edu.cn/download.html

ACKNOWLEDGMENTS

The work was funded by the National Natural Science Foundation of China(62106233), the Key Science and Technology Program of Henan Province(232102211003,232102210017)

REFERENCES

[1] X.R. Gao, Y.J. Wang, X.G. Chen, S.K. Gao, Interface, interaction, and intelligence in generalized brain-computer interfaces, Trends in Cognitive Sciences 25(8) (2021) 671-684.

[2] M.L. Martini, E.K. Oermann, N.L. Opie, F. Panov, T. Oxley, K. Yaeger, Sensor Modalities for Brain-Computer Interface Technology: A Comprehensive Literature Review, Neurosurgery 86(2) (2020) E108-E117.

[3] A. Craik, Y.T. He, J.L. Contreras-Vidal, Deep learning for electroencephalogram (EEG) classification tasks: a review, Journal of Neural Engineering 16(3) (2019).

[4] H. Altaheri, G. Muhammad, M. Alsulaiman, S.U. Amin, G.A. Altuwaijri, W. Abdul, M.A. Bencherif, M. Faisal, Deep learning techniques for classification of electroencephalogram (EEG) motor imagery (MI) signals: a review, Neural Computing & Applications 35(20) (2023) 14681-14722.

[5] Y. Zhang, S.N.Q. Xie, H. Wang, Z.Q. Zhang, Data Analytics in Steady-State Visual Evoked Potential-Based Brain-Computer Interface: A Review, Ieee Sensors Journal 21(2) (2021) 1124-1138.

[6] F. Marini, C. Lee, J. Wagner, S. Makeig, M. Gola, A comparative evaluation of signal quality between a research-grade and a wireless dry-electrode mobile EEG system, Journal of Neural Engineering 16(5) (2019).

[7] Y.M. Chi, T.-P. Jung, G. Cauwenberghs, Dry-contact and noncontact biopotential electrodes: methodological review, IEEE reviews in biomedical engineering 3 (2010) 106-19.

[8] A. Pourahmad, A. Mahnam, Evaluation of a Low-cost and Low-noise Active Dry Electrode for Long-term Biopotential Recording, Journal of medical signals and sensors 6(4) (2016) 197-202.

[9] A. Kübler, F. Nijboer, J. Mellinger, T.M. Vaughan, H. Pawelzik, G. Schalk, D.J. McFarland, N. Birbaumer, J.R. Wolpaw, Patients with ALS can use sensorimotor rhythms to operate a brain-computer interface, Neurology 64(10) (2005) 1775-1777.

[10] J.W.Y. Kam, S. Griffin, A. Shen, S. Patel, H. Hinrichs, H.J. Heinze, L.Y. Deouell, R.T. Knight, Systematic comparison between a wireless EEG system with dry electrodes and a wired EEG system with wet electrodes, Neuroimage 184 (2019) 119-129.

[11] H. Peng, B. Hu, Q.X. Shi, M. Ratcliffe, Q.L. Zhao, Y.B. Qi, G.P. Gao, Removal of Ocular Artifacts in EEG-An Improved Approach Combining DWT and ANC for Portable Applications, Ieee Journal of Biomedical and Health Informatics 17(3) (2013) 600-607.

[12] Q.L. Zhao, B. Hu, Y.J. Shi, Y. Li, P. Moore, M.H. Sun, H. Peng, Automatic Identification and Removal of Ocular Artifacts in EEG-Improved Adaptive Predictor Filtering for Portable Applications, Ieee Transactions on Nanobioscience 13(2) (2014) 109-117.

[13] B.N. Krupa, M.A.M. Ali, E. Zahedi, The application of empirical mode decomposition for the enhancement of cardiotocograph signals, Physiological Measurement 30(8) (2009) 729-743.

[14] M. Suchetha, N. Kumaravel, Empirical mode decomposition based filtering techniques for power line interference reduction in electrocardiogram using various adaptive structures and subtraction methods, Biomedical Signal Processing and Control 8(6) (2013) 575-585.

[15] X.Q. Chen, H.X. Chen, Y.S. Yang, H.F. Wu, W.H. Zhang, J.S. Zhao, Y. Xiong, Traffic flow prediction by an ensemble framework with data denoising and deep learning model, Physica a-Statistical Mechanics and Its Applications 565 (2021).

[16] Z. Wu, N.E. Huang, Ensemble Empirical Mode Decomposition: a Noise-Assisted Data Analysis Method, Adv. Data Sci. Adapt. Anal. 1 (2009) 1-41.

[17] J.-R. Yeh, J.S. Shieh, N.E. Huang, Complementary Ensemble Empirical Mode Decomposition: a Novel Noise Enhanced Data Analysis Method, Adv. Data Sci. Adapt. Anal. 2 (2010) 135-156.

[18] K. Dragomiretskiy, D. Zosso, Variational Mode Decomposition, IEEE Transactions on Signal Processing 62(3) (2014) 531-544.

[19] Y.J. Xue, J.X. Cao, D.X. Wang, H.K. Du, Y. Yao, Application of the Variational-Mode Decomposition for Seismic Time-frequency Analysis, Ieee Journal of Selected Topics in Applied Earth Observations and Remote Sensing 9(8) (2016) 3821-3831.

[20] W. Liu, S.Y. Cao, Z.M. Wang, X.Z. Kong, Y.K. Chen, Spectral Decomposition for Hydrocarbon Detection Based on VMD and Teager-Kaiser Energy, Ieee Geoscience and Remote Sensing Letters 14(4) (2017) 539-543.

[21] P. Pandey, K.R. Seeja, Subject independent emotion recognition from EEG using VMD and deep learning, Journal of King Saud University - Computer and Information Sciences 34(5) (2022) 1730-1738.

[22] A. Narmada, M.K. Shukla, A novel adaptive artifacts wavelet Denoising for EEG artifacts removal using deep learning with Meta-heuristic approach, Multimedia Tools and Applications 82(26) (2023) 40403-40441.

[23] Y. Liu, G. Yang, M. Li, H. Yin, Variational mode decomposition denoising combined the detrended fluctuation analysis, Signal Processing 125 (2016) 349-364.

[24] K. Zhang, B.P. Tang, L. Deng, X.L. Liu, A hybrid attention improved ResNet based fault diagnosis method of wind turbines gearbox, Measurement 179 (2021).

[25] R.Q. Yan, R.X. Gao, X.F. Chen, Wavelets for fault diagnosis of rotary machines: A review with applications, Signal Processing 96 (2014) 1-15.

[26] F. He, Q. Ye, A Bearing Fault Diagnosis Method Based on Wavelet Packet Transform and Convolutional Neural Network Optimized by Simulated Annealing Algorithm, Sensors 22(4) (2022).

[27] E. Alickovic, J. Kevric, A. Subasi, Performance evaluation of empirical mode decomposition, discrete wavelet transform, and wavelet packed decomposition for automated epileptic seizure detection and prediction, Biomedical Signal Processing and Control 39 (2018) 94-102.

[28] M. Mamun, M. Al-Kadi, M. Marufuzzaman, Effectiveness of Wavelet Denoising on Electroencephalogram Signals, Journal of Applied Research and Technology 11 (2013) 156-160.

[29] H.S.N. Murthy, M. Meenakshi, Ieee, Optimum Choice of Wavelet Function and Thresholding Rule for ECG Signal Denoising, International Conference on Smart Sensors and Systems (IC-SSS), Bangalore, INDIA, 2015.

[30] C. Kaur, A. Bisht, P. Singh, G. Joshi, EEG Signal denoising using hybrid approach of Variational Mode Decomposition and wavelets for depression, Biomedical Signal Processing and Control 65 (2021).

[31] Z. Lin, C. Zhang, W. Wu, X. Gao, Frequency recognition based on canonical correlation analysis for SSVEP-based BCIs, IEEE Trans Biomed Eng 53(12 Pt 2) (2006) 2610-4.

[32] C. Tong, H. Wang, C. Yang, X. Ni, Group ensemble learning enhances the accuracy and convenience of SSVEP-based BCIs via exploiting inter-subject information, Biomedical Signal Processing and Control 68 (2021).

[33] X. Chen, Y. Wang, S. Gao, T.-P. Jung, X. Gao, Filter bank canonical correlation analysis for implementing a high-speed SSVEP-based brain–computer interface, Journal of Neural Engineering 12(4) (2015).

[34] M. Nakanishi, Y.J. Wang, X.G. Chen, Y.T. Wang, X.R. Gao, T.P. Jung, Enhancing Detection of SSVEPs for a High-Speed Brain Speller Using Task-Related Component Analysis, Ieee Transactions on Biomedical Engineering 65(1) (2018) 104-112.

[35] F. Zhu, L. Jiang, G. Dong, X. Gao, Y. Wang, An Open Dataset for Wearable SSVEP-Based Brain-Computer Interfaces, Sensors (Basel) 21(4) (2021).

[36] W. Zhang, M. Zhang, Y. Zhao, B. Jin, W. Dai, Denoising of the Fiber Bragg Grating Deformation Spectrum Signal Using Variational Mode Decomposition Combined with Wavelet Thresholding, Applied Sciences 9(1) (2019).

[37] Liang, L.Y., Zhang, Q., Zhou, J., Li, W.Y., Gao, X.R., Dataset Evaluation Method and Application for Performance Testing of SSVEP-BCI Decoding Algorithm, Sensors 23(14) (2023).

[38] Zhang, X.Y. et al., Bidirectional Siamese correlation analysis method for enhancing the detection of SSVEPs, Journal of Neural Engineering 19(4) (2022).